

## Research Paper

# MRI/DTI of the Brain Stem Reveals Reversible and Irreversible Disruption of the Baroreflex Neural Circuits: Clinical Implications

Chia-Hao Su<sup>1\*</sup>, Ching-Yi Tsai<sup>1\*</sup>, Alice Y.W. Chang<sup>2</sup>, Julie Y.H. Chan<sup>1</sup>, Samuel H.H. Chan<sup>1</sup>✉

1. Institute for Translational Research in Biomedicine, Kaohsiung Chang Gung Memorial Hospital, Kaohsiung, Taiwan, Republic of China;
2. Institute of Physiology, National Cheng Kung University, Tainan, Taiwan, Republic of China.

\*Chia-Hao Su and Ching-Yi Tsai contributed equally to this work.

✉ Corresponding author: Samuel H.H. Chan, Institute for Translational Research in Biomedicine, Kaohsiung Chang Gung Memorial Hospital, Kaohsiung 83301, Taiwan, Republic of China. Tel: +88677317123. Fax: +88677317123. Email: shhchan@adm.cgmh.org.tw.

© Ivyspring International Publisher. Reproduction is permitted for personal, noncommercial use, provided that the article is in whole, unmodified, and properly cited. See <http://ivyspring.com/terms> for terms and conditions.

Received: 2015.12.29; Accepted: 2016.03.06; Published: 2016.04.11

## Abstract

Baroreflex is the physiological mechanism for the maintenance of blood pressure and heart rate. Impairment of baroreflex is not a disease per se. However, depending on severity, the eventuality of baroreflex dysfunction varies from inconvenience in daily existence to curtailment of mobility to death. Despite universal acceptance, neuronal traffic within the contemporary neural circuits during the execution of baroreflex has never been visualized. By enhancing signal detection and fine-tuning the scanning parameters, we have successfully implemented tractographic analysis of the medulla oblongata in mice that allowed for visualization of connectivity between key brain stem nuclei in the baroreflex circuits. When viewed in conjunction with radiotelemetric analysis of the baroreflex, we found that under pathophysiological conditions when the disrupted connectivity between key nuclei in the baroreflex circuits was reversible, the associated disease condition (e.g. neurogenic hypertension) was amenable to remedial measures. Nevertheless, fatality ensues under pathological conditions (e.g. hepatic encephalopathy) when the connectivity between key substrates in the baroreflex circuits was irreversibly severed. MRI/DTI also prompted partial re-wiring of the contemporary circuit for baroreflex-mediated sympathetic vasomotor tone, and unearthed an explanation for the time lapse between brain death and the inevitable asystole signifying cardiac death that follows.

Key words: Neuroimaging, Baroreflex-mediated vasomotor tone, Cardiac vagal baroreflex, Neural circuits, Neurogenic hypertension, Hepatic Encephalopathy, Brain death.

## Introduction

Perhaps the two most common physiological measurements in clinical practice are blood pressure (BP) and heart rate (HR), and the most fundamental mechanism for short-term [1] and long-term [2] regulation of BP and HR is the baroreflex. Based initially on anatomical (tracers), physiological (stimulation or lesion) and pharmacological (agonists and antagonists) methodologies [3, 4] and later on Fos expression [5], a well-established dogma of the baroreflex neural circuits stipulates that an increase in

nerve impulses in the primary baroreceptor afferents because of augmented BP detected by the arterial baroreceptors will lead to excitation of neurons in the nucleus tractus solitarius (NTS). From there, two physiological consequences will ensue to normalize BP. In cardiac vagal baroreflex, fibers from the NTS will excite neurons in the nucleus ambiguus (NA), which in turn reduces HR via the vagus nerve. Simultaneously, outputs from the NTS will elicit a baroreflex-mediated decrease in sympathetic

vasomotor tone by exciting the caudal ventrolateral medulla (CVLM), which in turn inhibits the rostral ventrolateral medulla (RVLM), a site that exerts a tonic excitatory action on the sympathetic preganglionic neurons in the thoracic spinal cord. Similarly, the opposite events will take place to normalize a reduction in BP. Impairment of baroreflex therefore inevitably results in a hypertensive or hypotensive state, and death in extreme cases [6].

Until recently [7], whether neuronal traffic in the above-mentioned circuits actually takes place in the brain stem during the execution of baroreflex has never been visualized. This is because unlike the forebrain, application of magnetic resonance imaging (MRI) and diffusion tensor imaging (DTI) to the brain stem, particular in mice, requires extraordinary efforts to enhance signal detection and fine tune the scanning parameters. Based on successful implementation of tractographic analysis of the medulla oblongata in mice, we report here that the prevalence of traffic within the neural circuits of cardiac vagal baroreflex and baroreflex-mediated sympathetic vasomotor tone bears clinical implications that are dependent on the physiological, pathophysiological and pathological conditions.

## Materials and Methods

### Ethics statement

All experimental procedures carried out in this study were approved by the Institutional Animal Care and Use Committee of the Kaohsiung Chang Gung Memorial Hospital, and were in compliance with the guidelines for animal care and use set forth by that committee.

### Animals

Male adult C57BL/6 mice ( $26 \pm 3$  g) purchased from the Experimental Animal Center of the Ministry of Science and Technology, Taiwan were used. Animals were housed in an AAALAC International-accredited Center for Laboratory Animals under temperature control (24–25°C) and 12-h light-dark cycle (lights on at 07:00 h). Standard laboratory rat chow and tap water were available ad libitum.

### MRI and DTI

Sequential MRI/DTI acquisition was performed under isoflurane anesthesia in a 9.4T horizontal-bore animal MR scanning system (Biospec 94/20, Bruker, Ettingen, Germany). This scanning system is made up of a self-shielded magnet with a 20-cm clear bore and a BGA-12S gradient insert (12-cm inner diameter) that offered a maximal gradient strength of  $675 \text{ mT m}^{-1}$  and a minimum slew rate of  $4673 \text{ Tm}^{-1}\text{s}^{-1}$ . It is also equipped with a modified high performance

transmitter-receiver surface cryo-probe coil for signal detection from the head of the mouse. As a routine, high resolution  $T_2$ -weighted sagittal anatomical reference images were first recorded, using multislice turbo rapid acquisition with refocusing echoes (Turbo-RARE) sequence. Based on orientation of landmark structures from the sagittal images (Supplementary Table 1),  $T_2$ -weighted coronal anatomical reference imaging was performed on 10 adjacent slices from a restricted area of the brain stem that covered the medullary portion of the NTS, NA, RVLM and CVLM using Turbo-RARE sequence acquisition (Supplementary Table 2). Employing identical spatial dimension as in the  $T_2$ -weighted coronal reference imaging, the connectivity between those key brain stem nuclei in the circuits of cardiac vagal baroreflex or baroreflex-mediated sympathetic vasomotor tone was subsequently evaluated using the spin echo-planar imaging-DTI sequence in the coronal plane covering the same ten  $200\text{-}\mu\text{m}$  slices without gap (Supplementary Table 3). We chose a slice thickness of  $200 \mu\text{m}$  and an in-plane voxel dimension of  $94 \mu\text{m}$  for this sequence because they provided the optimal condition for our tractographic evaluation of the brain stem. In preliminary experiments, by reducing the slice thickness to  $100 \mu\text{m}$  and increasing the number of slice to 20, the repetition time was increased from 2500 ms to 5000 ms, the acquisition time from 33 min 45 s to 67 min 30 s, and the signal-to-noise ratio was decreased from 25 to 10.

### Post-processing of images

Post-processing of the image data entailed an analysis of fiber tractography and determination of DTI indices, using the National Taiwan University DSI studio (<http://dsi-studio.labsolver.org>). At each time-point, the fiber tracts between the NTS and NA or the NTS and RVLM on both sides were selected for tractographic evaluation. In addition, regions-of-interest (ROIs)-based analysis was performed to quantify two DTI indices, fractional anisotropy (FA) and number of fiber tracts [8]. Values of FA, which ranged from 0 (isotropy) to 1 (maximum anisotropy), were derived from the standard deviation of the three eigenvalues ( $\lambda_1, \lambda_2, \lambda_3$ ) of the diffusion ellipse of probability density function. Representative colors for tractography in color-encoded FA maps were: blue, caudal-rostral; red, left-right; and green, dorsal-ventral. We also measured axial diffusivity ( $\lambda_{\parallel}$ ) and radial diffusivity ( $\lambda_{\perp}$ ) to determine the main eigenvalues of water diffusion in the brain stem. To calculate fiber numbers, the tracts that passed through both NTS and NA or NTS and CVLM or RVLM were counted using the streamline tracking method.

### **Animal model of neurogenic hypertension**

Intracerebroventricular (i.c.v.) infusion of angiotensin II (Ang II) (Sigma-Aldrich, St. Louis, MO, USA) [7] was delivered by an osmotic minipump (Alzet1007D; Alzet Corp, Cupertino, CA, USA) for 7 days at 7.5 µg/h and a rate of 0.5 µL/h. The dose of Ang II used was the same as in our previous study [7]. Lowering the dose to half in preliminary experiments resulted in inconsistent responses in our experimental indices.

### **Animal model of hepatic encephalopathy (HE)**

A single intraperitoneal injection of azoxymethane (AOM; 100 µg/g) was delivered to induce acute liver failure [9, 10]. Animals were evaluated for prominent neurobehavioral changes according to the classifications by the West Haven scale [11, 12].

### **Blood pressure and heart rate recording by radiotelemetry and determination of spontaneous baroreflex**

Similar to our previous study [7, 13], BP of animals was recorded by radiotelemetry under a conscious state in their home cages using telemeters (TA11PA-C10; Data Sciences International, Minneapolis, MN, USA) that were surgically implanted 14 days before commencement of the experiment. The transmitted BP signals were digitized and processed by an arterial blood pressure analyzer (APR31a, Notocord Systems, Croissy-Sur-Seine, France) based on feature extraction to detect and measure the characteristics of BP cycles. Systolic blood pressure (SBP), mean arterial pressure (MAP) and HR were derived from the BP waveforms on a beat-by-beat basis.

Continuous, on-line and real-time auto-spectral analysis (SPA10a, Notocord) of SBP signals was used to detect temporal fluctuations of the low-frequency (BLF; 0.15-0.6 Hz) component in the SBP spectrum [7]. We demonstrated previously [14] that the power density of this spectral band is a valid index for baroreflex-mediated sympathetic vasomotor tone. To evaluate the cardiac vagal baroreflex, we employed a baroreflex sequence analyzer (BRS10a, Notocord) to determine baroreflex sensitivity (BRS) based on on-line detection of spontaneous sequences of consecutive increases or decreases in SBP associated with parallel changes in HR [15]. Concurrent 24-h changes in SBP, MAP, HR, power density of the BLF band, BRS and activity of the animals were continuously recorded. The averaged values of those parameters recorded between 11:00 and 15:00 daily in the neurogenic hypertension model, or every hour in the HE model, were taken to represent the daily or

hourly results.

### **Blood chemistry**

Blood samples for measurement of aspartate aminotransferase (AST), alanine aminotransferase (ALT), total bilirubin (T-Bilirubin), or albumin were taken before and after AOM administration. Approximately 0.2 ml of blood sample was centrifuged at 2000 g for 15 min. The serum levels of AST, ALT, T-Bilirubin, or albumin were determined by an autoanalyzer (Fujifilm, Tokyo, Japan).

### **Reactive oxygen species (ROS)/reactive nitrogen species (RNS) assay**

Total ROS/RNS in NTS or RVLM tissue was measured by a ROS/RNS assay kit (Cell Biolabs, San Diego, CA, USA) according to the manufacturer's protocol. Fluorescence intensity, which is proportional to the total ROS/RNS levels within the sample, was read at 480 nm excitation/530 nm emission in a fluorescence plate reader (Gemini EM; Molecular Devices, Sunnyvale, CA, USA).

### **Histological examination**

The liver and brain stem were removed immediately after sacrifice and fixed in 10% neutral-buffered formalin for 24 h. The tissues were dehydrated, embedded in paraffin, sectioned at 4 µm thickness, and stained by hematoxylin and eosin (H&E) for histopathological examination.

### **Statistical analysis**

All values are expressed as means ± SEM. One-way or two-way analysis of variance with repeated measures was used to assess the group means, as appropriate, followed by the Dunnett multiple-range test for post hoc assessment of the individual means.  $P < 0.05$  was taken to indicate statistical significance.

## **Results**

### **Visualization of connectivity between key brain stem nuclei in the baroreflex circuits in mice**

Tractographic analysis of the baroreflex neural circuits, particularly in mice, requires extraordinary efforts to fine tune the scanning parameters because of the size of the brain stem. Employing a 9.4T horizontal-bore animal MR scanning system equipped with a cryo-probe coil (Figure 1), we were able to visualize the connectivity between key brain stem nuclei in the baroreflex circuits in mice. This was achieved via systematic optimization of the scanning parameters for T<sub>2</sub>-weighted sagittal anatomical reference imaging of the brain (Supplementary Table 1), coronal anatomical imaging of a restricted brain

stem area that contains the medullary portion of NTS, NA, RVLM or CVLM (Supplementary Table 2), and imaging the connectivity between these medullary nuclei using spin echo-planar imaging-DTI sequence (Supplementary Table 3). When viewed in conjunction with changes in BP, HR, and indices of cardiac vagal baroreflex or baroreflex-mediated sympathetic vasomotor tone obtained by radiotelemetry coupled with power spectral analysis (Figure 1), these tractographic data revealed reversible and irreversible alterations of the baroreflex neural circuits that bear important clinical implications. Visualization of the connectivity between key brain stem nuclei also prompted partial re-wiring of the contemporary circuit for baroreflex-mediated sympathetic vasomotor tone, and unearthed an explanation for the time lapse between brain death and the inevitable cardiac death that follows.

### Neurogenic hypertension: A case of pathophysiological changes in baroreflex because of reversible disruption of functional connectivity between key brain stem nuclei in the neural circuits

Neurogenic hypertension refers to a chronic hypertensive state that is not induced by defects of peripheral organs or blood vessels, but is consequential to depressed baroreflex. A well-established animal model for neurogenic hypertension [7] entailed i.c.v. infusion of Ang II by osmotic minipump (Figure 1). In male adult C57BL/6 mice instrumented for physiological measurements by

radiotelemetry under conscious conditions in their home cage (Figure 1), i.c.v. infusion of Ang II ( $7.5 \mu\text{g}/\text{h}$  at  $0.5 \mu\text{L}/\text{h}$ ) for 7 days elicited a significant elevation in MAP or HR and reduction in physical activity (Days 2 and 7; Figure 2b,d) that returned to basal levels over time (Day 21; Figure 2b,d). Determined by the slope method and presented as the spontaneous BRS [7, 13, 15], the cardiac vagal baroreflex underwent a significant reduction that mirrored temporally the increase in HR (Figure 2b,d). Likewise, determined by the power density of the BLF component of the SBP spectrum [13, 15, 16], the baroreflex-mediated sympathetic vasomotor tone exhibited a significant increase that paralleled temporally the elevation in MAP (Figure 2b,d).

Tractographic analysis based on MRI/DTI of the medulla oblongata further revealed that under basal SBP and HR, there was robust connectivity between the NTS and NA or NTS and RVLM. Both NTS-NA and NTS-RVLM connectivity was substantially reduced (Days 2 and 7; Figure 2a) when visualized during sustained hypertension or tachycardia and depressed cardiac vagal baroreflex or baroreflex-mediated sympathetic vasomotor tone. More importantly, the connectivity between the NTS and NA or NTS and RVLM (Day 21; Figure 2a) was re-established when MAP, HR, BRS or BLF power returned to their basal levels (Figure 2b). Quantification of the magnitude of NTS-NA or NTS-RVLM connectivity by two DTI indices yielded comparable results. The temporal changes in the

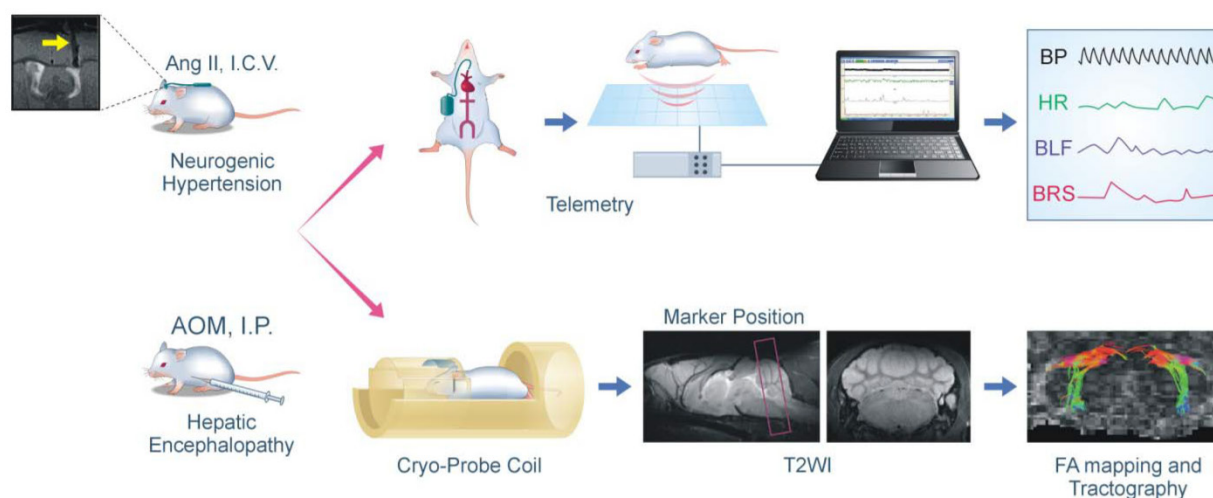


**Figure 1. Flowchart of the experimental setup and procedures for MRI/DTI and radiotelemetry in conjunction with neurogenic hypertension and hepatic encephalopathy.** In the neurogenic hypertension model, mice received intracerebroventricular (I.C.V.) infusion of angiotensin (Ang II) by osmotic minipump via a MRI confirmed implantation of cannula into the lateral ventricle (yellow arrow). In the hepatic encephalopathy model, mice received intraperitoneal (I.P.) administration of azoxymethane (AOM). These mice may also be instrumented for radiotelemetric recording of their blood pressure under conscious state in their home cage; and the computer processed cardiovascular parameters, including indices for the baroreflex, were displayed continuously. In association with a cryo-probe, these mice may also be subjected first to high resolution T<sub>2</sub>-weighted sagittal anatomical reference image to demarcate the area of the brain stem for tractographic analysis with DTI. This was followed by T<sub>2</sub>-weighted coronal anatomical reference image showing locations of the key sites in the baroreflex neural circuits. Finally, fractional anisotropy (FA) maps of the brain stem were generated, and were used to quantify the DTI indices on the connectivity between those key sites.

respective FA and number of fiber tracts (Figure 2c) paralleled those of the cardiac vagal baroreflex (Figure 2d) or mirrored the baroreflex-mediated sympathetic vasomotor tone (Figure 2d), and were accompanied by changes in tissue levels of ROS/RNS in the NTS or RVLM that also exhibited a mirror-image pattern (Figure 2d). Likewise, the significant reduction in  $\lambda_{||}$  in the brain stem on Days 2 and 7 returned to baseline level on Day 21 (Table 1), without significant changes in  $\lambda_{\perp}$  at all time-points evaluated. As a negative control, on the other hand, tractographic analysis of the bilateral pyramidal tracts, which do not play a role in cardiac vagal baroreflex or baroreflex-mediated sympathetic vasomotor tone, showed consistent DTI images and FA values only in the caudal-rostral direction (Figure 4a) before, during and after i.c.v. infusion of Ang II.

**Table 1.** Axial diffusivity ( $\lambda_{||}$ ) and radial diffusivity ( $\lambda_{\perp}$ ) values in the brain stem of mice after infusion of angiotensin II (Ang II).

	Brain Stem	
	$\lambda_{  }$ ( $\times 10^{-4}$ mm <sup>2</sup> /s)	$\lambda_{\perp}$ ( $\times 10^{-4}$ mm <sup>2</sup> /s)
Basal	9.40 $\pm$ 0.14	6.52 $\pm$ 0.12
Ang II Day 2	7.51 $\pm$ 0.28*	6.21 $\pm$ 0.13
Ang II Day 7	7.58 $\pm$ 0.26*	6.20 $\pm$ 0.11
Ang II Day 21	9.40 $\pm$ 0.25	6.53 $\pm$ 0.16

Values are mean  $\pm$  SEM, n = 7 animals per group. \*P < 0.05 versus pre-infusion control (Basal) group in the post hoc Dunnett multiple-range analysis.

### Hepatic encephalopathy: A case of pathological changes in baroreflex because of irreversible disruption of functional connectivity between key brain stem nuclei in the neural circuits

HE is most commonly seen in patients with advanced liver cirrhosis and severe hepatocellular dysfunction [17, 18]. In acute hepatic failure, the onset of encephalopathy is an indication for liver transplantation [19], without which results in 50–90% mortality [20]. Male adult C57BL/6 mice that received a single intraperitoneal injection of AOM (100  $\mu$ g/g) exhibited typical clinical markers of liver damage, including a significant and progressive increase in serum levels of AST, ALT, T-Bilirubin or albumin (Supplementary Table 4), along with necrotic cell death and neutrophil infiltration in the liver (Supplementary Figure 1). All animals died within 24–30 h after AOM administration.

Results from radiotelemetry (Figure 3b,d) revealed a significant increase in physical activity at 2 h, followed by a progressive decline typically exhibited by patients with HE. HR was maintained and even elevated during the first 12 h, followed by a significant decrease to a level that was sustained until

the abrupt occurrence of asystole around 24 h signifying cardiac death (Figure 3b, fine dotted line). As reflected by the spontaneous BRS, cardiac vagal baroreflex persisted until shortly before the abrupt occurrence of cardiac arrest despite a significant depression that began at 12 h. MAP underwent a significant increase (2 h) followed by a decrease that began at 12 h, approaching zero around 24 h. Intriguingly, the power density of the BLF component in the SBP spectrum already underwent drastic reduction that began at 12 h. This index of baroreflex-mediated sympathetic vasomotor tone reached zero (Figure 3b, gross dotted line) before the occurrence of asystole. Clinically, this signifies brain death in comatose patients despite the presence of reasonable SBP and maintained HR [21–23].

Tractographic analysis of the brain stem again revealed that the temporal changes in connectivity between the NTS and NA (Figure 3a) during the course of HE manifested a trend that resembled that of the spontaneous BRS (Figure 3d). The robust NTS-NA connectivity was maintained during the first 2 h, to be followed by a reduction at 12 h. Complete disruption of the connectivity between the NTS and NA only took place towards the end of the 24-h observation period. Likewise, the temporal changes in connectivity between the NTS and RVLM (Figure 3a) during experimental HE manifested a trend that resembled that of the power density of the BLF component of SBP spectrum (Figure 3d). Of note is that the NTS-RVLM connectivity was eliminated beginning at 12 h, without returning at 24 h, coincidental with the significant reduction in baroreflex-mediated sympathetic vasomotor tone. Again, quantification by FA and number of fiber tracts revealed comparable results (Figure 3c). There was also a significant reduction in  $\lambda_{||}$  in the brain stem at 12 h after AOM treatment, with further decrease at 24 h (Table 2), although changes in  $\lambda_{\perp}$  were insignificant. Biochemical data showed a trend of elevated ROS/RNS in the NTS, reaching significance at 24 h for NTS. On the other hand, significant increase in ROS/RNS was already detected in the RVLM at 12 h (Figure 3d). Morphologically, damaged neurons characterized by shrunken cell body, intensive eosinophilic cytoplasm, and pyknotic nucleus that lacks discernible nucleolus were found in both NTS and RVLM at 24 h (Supplementary Figure 2). In addition, as a negative control, tractographic analysis of the bilateral pyramidal tracts (Figure 4b) showed consistent DTI images and FA values only in the caudal-rostral direction during the course of experimental HE.

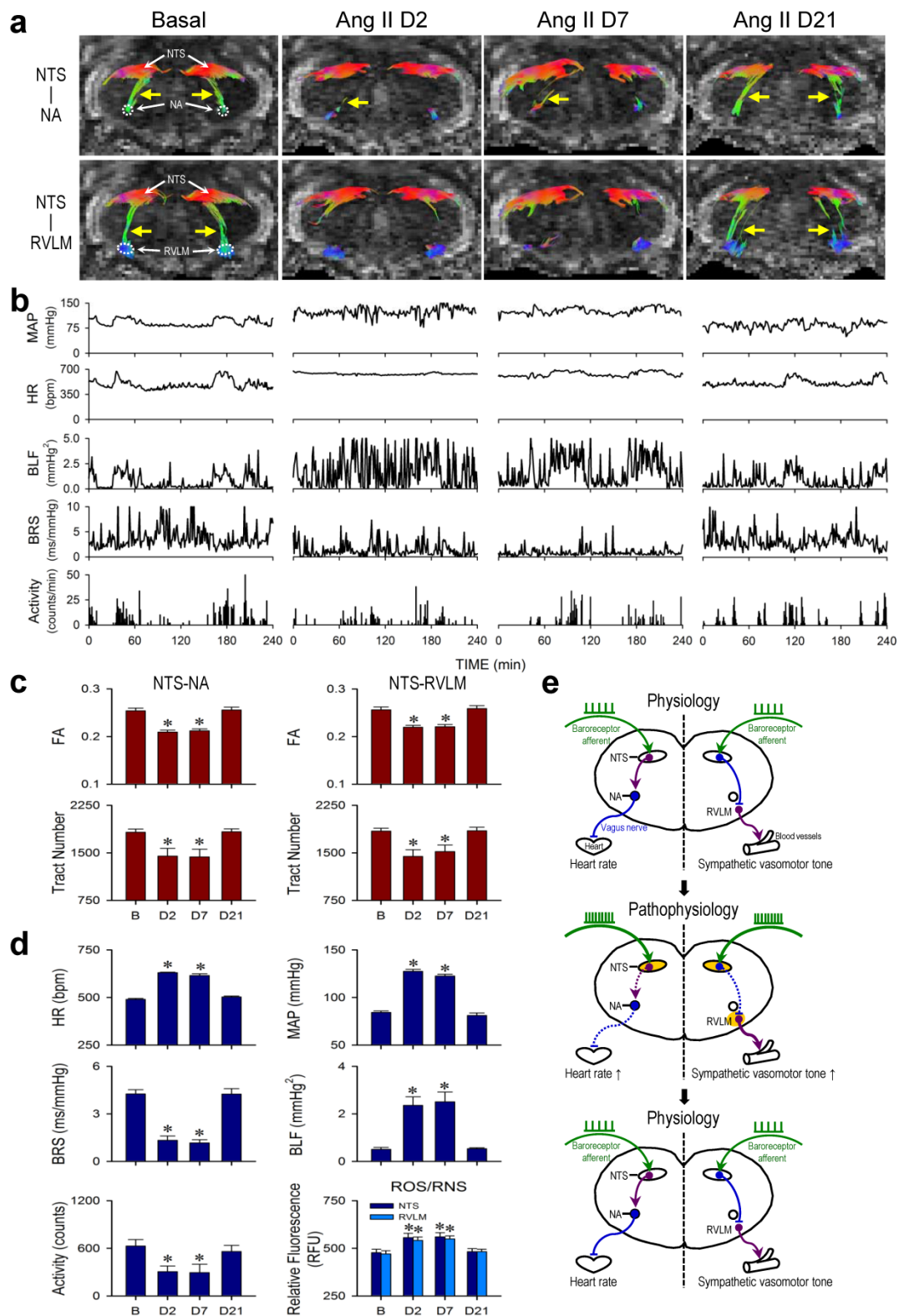


**Figure 2. Reversible disruption of baroreflex neural circuits in neurogenic hypertension.** (a,b) Illustrative examples of imaging connectivity between the NTS and NA or RVLM by DTI (a) or mean arterial pressure (MAP), heart rate (HR), power density of the low-frequency (BLF) component of the SBP spectrum, an index for baroreflex-mediated sympathetic vasomotor tone, baroreflex sensitivity (BRS), an index for cardiac vagal baroreflex, or physical activity measured by radiotelemetry (b) in mice before (Basal), during (Day 2 or Day 7) and after (Day 21) I.C.V. infusion of Ang II for 7 days. Note that in this and Figure 3, representative colors for tractography in color-encoded FA maps are: blue, caudal-rostral; red, left-right; and green, dorsal-ventral. (c,d) Temporal changes in FA or number of tracts connecting the NTS and NA or RVLM, quantitative indices for the magnitude of connectivity in DTI analysis (c), the cardiovascular parameters and activity, or tissue levels of reactive oxygen species/reactive nitrogen species (ROS/RNS) in the NTS or RVLM (d) during neurogenic hypertension. Values in (c,d) are mean ± SEM, n = 7 animals per group. \*P < 0.05 versus pre-infusion control (B) group in the post hoc Dunnett multiple-range analysis. (e) Diagrammatic illustration of the pathophysiological changes in baroreflex because of reversible disruption of connectivity between key brain stem nuclei in the neural circuits during neurogenic hypertension. Note resumption of physiological condition and connectivity when the impending condition of oxidative stress (shaded in yellowish brown) in the NTS or RVLM was removed. Solid line denotes connectivity, dashed line denotes disrupted connectivity, arrow head denotes excitation, and “⊥” denotes inhibition.

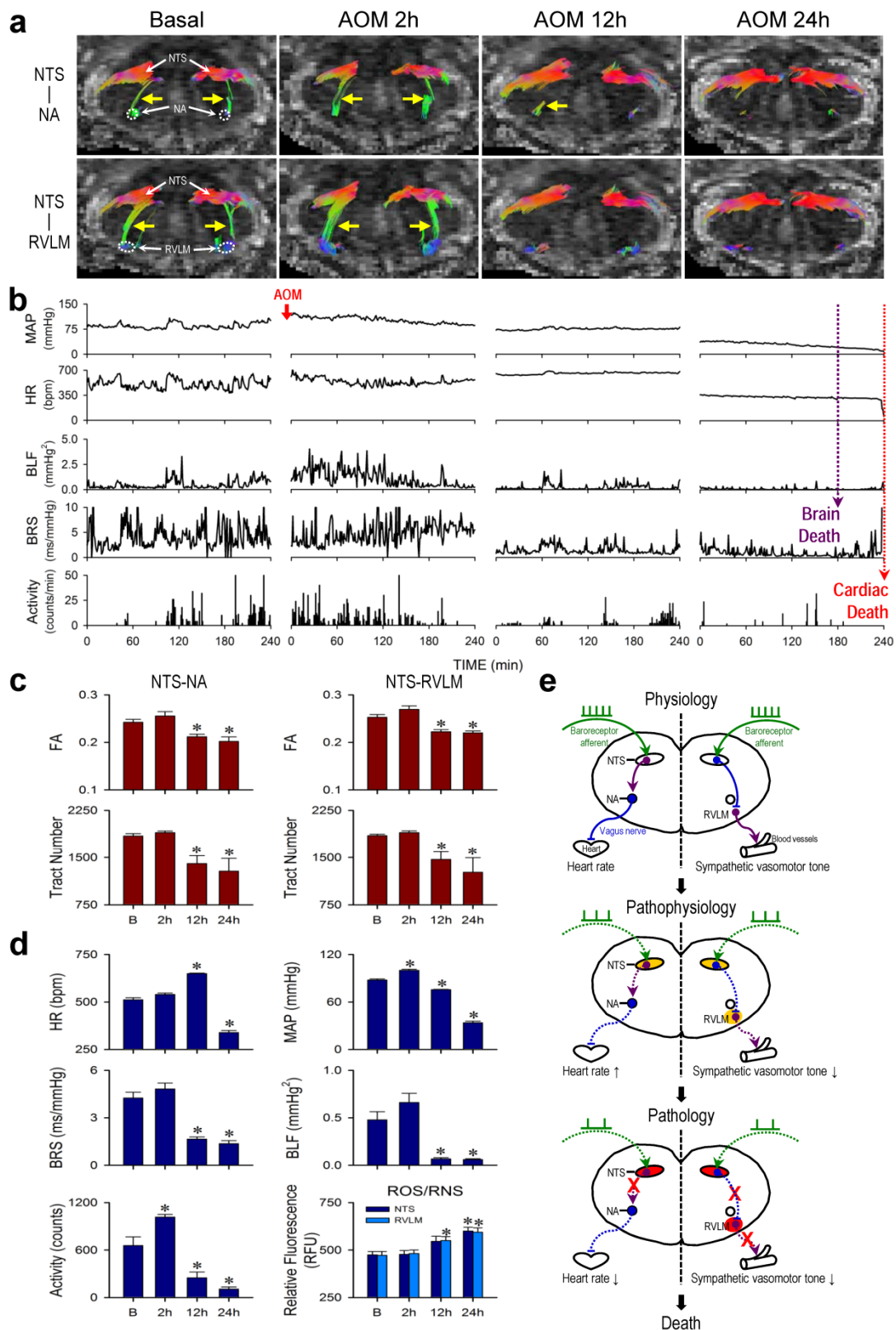


**Figure 3. Irreversible disruption of baroreflex neural circuits in hepatic encephalopathy.** (a,b) Illustrative examples of imaging connectivity between the NTS and NA or RVLM by DTI (a) or MAP, HR, power density of the BLF component of the SBP spectrum, BRS or physical activity measured by radiotelemetry (b) in mice before (Basal) and 2, 12 or 24 h after I.P. administration of AOM. (c,d) Temporal changes in FA or number of tracts connecting the NTS and NA or RVLM (c), the cardiovascular parameters and activity, or tissue levels of ROS/RNS in the NTS or RVLM (d) during hepatic encephalopathy. Values in (c,d) are mean  $\pm$  SEM, n = 7 animals per group. \*P < 0.05 versus pre-injection control (B) group in the post hoc Dunnett multiple-range analysis. (e) Diagrammatic illustration of the progression from pathophysiological to pathological changes in baroreflex because of irreversible disruption of connectivity between key brain stem nuclei in the neural circuits during hepatic encephalopathy. Note the progressive shift of oxidative stress (shade in yellowish brown) to nitrosative stress (shade in red) in the NTS or RVLM during this process. Solid line denotes connectivity, dashed line denotes disrupted connectivity, "X" denotes severed connectivity, arrow head denotes excitation, and "⊥" denotes inhibition.

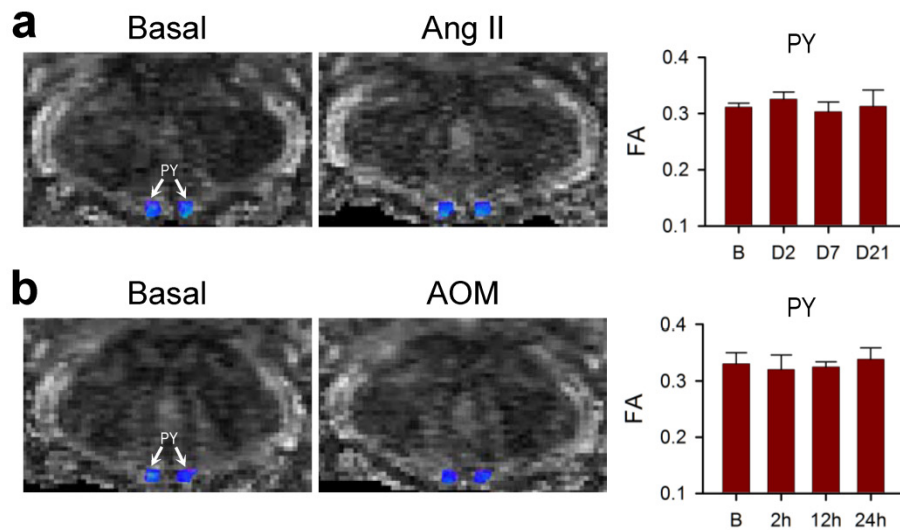


**Figure 4. Lack of effects on connectivity in the pyramidal tracts during neurogenic hypertension and hepatic encephalopathy.** (a,b) Illustrative example of imaging the bilateral pyramidal tracts (PY) in mice by DTI or the associated temporal changes in FA, quantitative index for the magnitude of connectivity in tractographic analysis, before (Basal or B), during (days 2 or 7) or after (day 21) intracerebroventricular infusion of Ang II to induce neurogenic hypertension (a); or before (Basal or B) and after (2, 12 or 24 h) intraperitoneal administration of AOM (b). Values of FA in (a,b) are mean  $\pm$  SEM, n = 7 animals. No statistical significance among all groups ( $P > 0.05$ ) in two-way ANOVA with repeated measures. Note consistent presence of caudal-rostral connectivity coded in blue, and the lack of dorsal-ventral connectivity coded in green.

**Table 2. Axial diffusivity ( $\lambda_{||}$ ) and radial diffusivity ( $\lambda_{\perp}$ ) values in the brain stem of mice after administration of azoxymethane (AOM).**

	Brain Stem	
	$\lambda_{  }$ ( $\times 10^{-4}$ mm <sup>2</sup> /s)	$\lambda_{\perp}$ ( $\times 10^{-4}$ mm <sup>2</sup> /s)
Basal	9.40 $\pm$ 0.15	6.52 $\pm$ 0.14
AOM 2h	9.42 $\pm$ 0.23	6.61 $\pm$ 0.17
AOM 12h	8.74 $\pm$ 0.17*	6.49 $\pm$ 0.10
AOM 24h	6.85 $\pm$ 0.49*	5.99 $\pm$ 0.31

Values are mean  $\pm$  SEM, n = 7 animals per group. \* $P < 0.05$  versus pre-infusion control (Basal) group in the post hoc Dunnett multiple-range analysis.

### Absence of connectivity between NTS and CVLM

The contemporary dogma stipulates that the CVLM participates in baroreflex-mediated sympathetic vasomotor tone by acting as a synaptic relay that connects the NTS to the RVLM. Functionally, CVLM exerts an inhibitory action on RVLM neurons involved in the tonic and reflex control of sympathetic vasomotor tone (Figure 5c) [3-5]. Interestingly, in an anterior-posterior presentation of the FA map of the medulla oblongata, we rarely ( $P < 0.0001$ , Chi-square analysis) detected the obligatory presence of connectivity between NTS and CVLM under basal conditions (3 out of 56 observations) or during neurogenic hypertension (1 out of 28 observations) or HE (2 out of 28 observations). Nevertheless, commensurate temporal changes in NTS-RVLM connectivity and baroreflex responses depicted in Figs. 2 and 3 were continuously manifested (Figure 5a,b). Our visualization of the baroreflex at work therefore necessitates partial

re-wiring of the circuit for baroreflex-mediated sympathetic vasomotor tone (Figure 5c).

## Discussion

### Visualizing the baroreflex neural circuits in brain stem is now feasible

This is the first time when tractographic analysis of the neural circuits of cardiac vagal baroreflex and baroreflex-mediated sympathetic vasomotor tone in the mouse medulla oblongata became feasible. Whereas MRI/DTI of the forebrain has been published extensively, application of this technique to the brain stem, particularly in mice, has been dearth. One obvious reason is the size of the mouse brain stem. In addition, the location of the brain stem beneath the cerebellum and in an oblique position from the horizontal plane of the cortical surface makes its accessibility by MRI difficult. One approach, as suggested by Kim and Song [24], is to apply an angled restraining device to the head of the mouse to produce an angle between the brain stem/cervical spinal cord and the rest of the mouse body. Since this is not a natural position for the mouse and would exert extra stress on the animal, we have resorted to placing the cortex in its horizontal position but improved signal detection from the head of the mouse by using a high performance transmitter-receiver surface cryo-probe coil. Together with systematic optimization of the scanning parameters, we were able to obtain high quality T<sub>2</sub>-weighted sagittal anatomical reference images of the brain, coronal anatomical images of the medulla oblongata, and DTI images of the connectivity between key components of the

baroreflex circuits. More importantly, when viewed in conjunction with our physiological indices, our tractographic data revealed that whether alterations of the baroreflex neural circuits are reversible or irreversible bear important clinical implications.

Our study design was based on the fundamental premise that DTI uses diffusion of water molecules as the probe to offer two pieces of information, diffusion anisotropy and fiber orientation, and tractographic analysis can be used to investigate brain connectivity. We reasoned that since the passage of action potentials along the axon will create prominent anisotropy, a decrease in FA can be taken to infer reduction or cessation of impulse traffic between two brain structures, which we termed disruption or severance of functional connectivity. Importantly, the significant reduction in  $\lambda_{\parallel}$  and the insignificant changes in  $\lambda_{\perp}$  measured in the brain stem during neurogenic hypertension and experimental HE further ascertained that the disrupted NTS-NA or NTS-RVLM connectivity revealed by our

tractographic analysis is restricted to water diffusion in the dorsal-ventral direction, the trajectory of the fiber tracks that connect the NTS and NA or the NTS and RVLM.

### Why study the baroreflex and brain stem?

We are cognizant that the baroreflex and brain stem are not limelight study subjects despite their vital importance. Whereas contemporary medical research places major emphasis on molecular and cellular information, one often forgotten fact is that BP and HR are most probably the first two primary vital signs measured from a patient. As the fundamental mechanism responsible for the maintenance of BP and HR, the eventuality of impairment of baroreflex may vary from inconvenience in daily existence to serious curtailment of mobility to death. Another often forgotten fact is that the functionality of the brain stem, not the forebrain, defines life-and-death [3]. Although patients in a persistent vegetative state (PVS) because of supratentorial lesions suffer from the worse degree of functional brain damage compatible with

prolonged survival [25] and display no awareness of external stimuli, the Multi-Society Task Force on PVS [26, 27] stipulates that their vital vegetative functions such as maintained BP and cardiac action are preserved. On the other hand, the importance of the brain stem to brain death is reflected in two memoranda issued by the Conference of Medical Royal Colleges and their Faculties in the UK. The first one [28], issued in 1976, emphasizes “permanent functional death of the brain stem constitutes brain death”. The second memorandum [29], issued in 1979, identifies brain stem death with death itself. Previous work from our laboratory also demonstrated that defunct baroreflex is causally related to brain death [6, 21-23], and whether cardiopulmonary resuscitation is successful depends on whether brain death has ensued in the subject [30]. It follows that studying the baroreflex and brain stem is of vital importance.

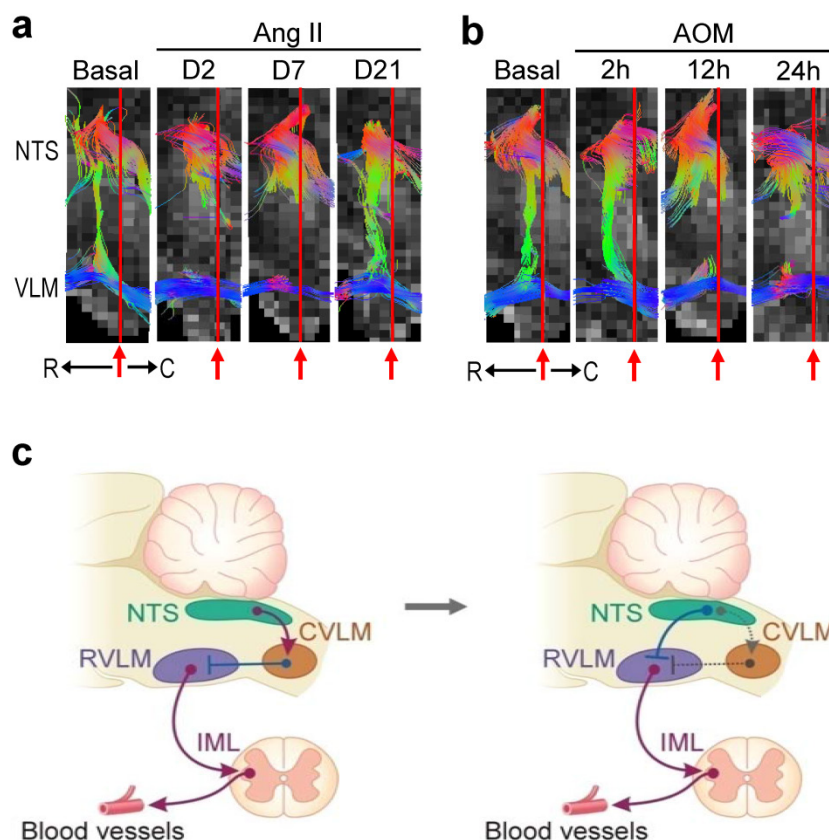


**Figure 5. Partial re-wiring of the contemporary baroreflex neural circuit.** (a,b) Illustrative examples of imaging connectivity between the NTS and the rostral (R) or caudal (C) ventrolateral medulla (VLM) by an anterior-posterior presentation of the FA map of the medulla oblongata in the neurogenic hypertension (a) or hepatic encephalopathy (b) model. (c) CVLM as an intermediate between the NTS and RVLM in the neural circuit for baroreflex-mediated sympathetic tone depicted in the classical literature (left side). An inhibitory input directly from the NTS to RVLM that in turn lessens the tonic excitatory action of these premotor sympathetic neurons on vasomotor tone in the re-wired circuit as revealed by DTI (right side). Solid line denotes connectivity, dashed line denotes putative non-existent connectivity, arrow head denotes excitation, and “⊥” denotes inhibition. IML, intermediolateral column where preganglionic sympathetic neurons are located.

### **MRI/DTI of the brain stem necessitates partial re-wiring of the contemporary neural circuit for baroreflex-mediate sympathetic vasomotor tone**

One surprising finding from visualization of the baroreflex at work is the almost lack of connectivity detected between the NTS and CVLM under basal conditions and during neurogenic hypertension or HE. On the other hand, there were prominent temporal alterations in functional connectivity between the NTS and RVLM that were commensurate with the time-course changes in baroreflex-mediated sympathetic vasomotor tone under the same experimental conditions. Those findings therefore necessitate partial re-wiring of the circuit that includes CVLM as an intermediate between the NTS and RVLM depicted in the classical literature [4] (Figure 5c, left side). Direct projection of barosensitive neurons in the NTS to the RVLM has been reported [5], as is the possibility for those NTS neurons to synapse with GABAergic interneurons in the RVLM [31]. As such, it is conceivable that the baroreflex-mediated sympathetic vasomotor tone of mice in our study is sustained by a tonic inhibitory input from the NTS to RVLM, which in turn lessens the tonic excitatory action of these premotor sympathetic neurons on vasomotor tone (Figure 5c, right side).

### **Unearthing an explanation for the time lapse between brain death and cardiac death**

In a series of articles on brain death commissioned by the *British Medical Journal* [32], Pallis pointed out succinctly that “brain stem death is the physiological kernel of brain death, the anatomical substratum of its cardinal signs (apnoeic coma with absent brain stem reflexes), and the main determinant of its invariable prognosis: asystole within hours or days”. The presence of an interim when cardiac functions are sustained after brain death until the invariable asystole (cardiac death) takes place is one of the driving forces for recognizing brain death as the legal definition of death in the US, UK and many other countries [32-36]. This time-window is vitally important for transplantation, which requires organ(s) retrieved from the donor to be in a relatively functional condition. Our results from MRI/DTI and radiotelemetry provided direct evidence to support the notion that unceasing cardiac vagal baroreflex because of the sustained connectivity between the NTS and NA, leading to the preservation of cardiac functions, is responsible for the vital period between brain death and the abrupt occurrence of cardiac death that inevitably follows.

### **Clinical implications**

Operated under physiological conditions (Figs. 2e and 3e), the cardiac vagal baroreflex and baroreflex-mediated sympathetic vasomotor tone are responsible for the maintenance of BP and HR [3]. Nonetheless, as exemplified by neurogenic hypertension (Figure 2e), a pathophysiological condition (increase in HR, sympathetic vasomotor tone and BP) is created when the connectivity between the NTS and NA and between the NTS and RVLM is disrupted because of oxidative stress induced by Ang II in the NTS and RVLM [7, 37, 38]. Intriguing, the disrupted connectivity is reversed when the impending oxidative stress is no longer present (Day 21) or when antioxidant is applied to the NTS [7] or RVLM (data not shown), resulting in the resumption of physiological condition when HR, BP and cardiac vagal baroreflex and baroreflex-mediated sympathetic vasomotor tone return to baseline. In addition to BP, central administration of Ang II is known to induce drinking and salt appetite [39, 40], and to suppress food intake [41, 42]. Whether those Ang II-induced effects may impact on our results remained to be investigated because our experimental design did not call for their measurement. Suffice to say, water intake elicited by i.c.v. Ang II has been reported to be inversely related to changes in MAP in the absence of sinoaortic baroreceptor input [43]. It follows that our observed changes in MAP and baroreflex in our model of neurogenic hypertension may bear minimal interactions with i.c.v. Ang II-induced drinking responses.

Under pathological conditions, defunct baroreflex has been demonstrated to be causally related to brain death in comatose patients [6, 21-23], and animal models of organophosphate poisoning [30, 44-48], endotoxemia [49-52], or fatal methamphetamine intoxication [53, 54]. Intriguingly, nitrosative stress induced by peroxynitrite formed by a reaction between nitric oxide and superoxide in key nuclei of the baroreflex circuits is identified as the culprit [54]. As exemplified by HE (Figure 3e), a pathophysiological condition (decrease in HR, sympathetic tone and BP) is created when the connectivity between the NTS and RVLM is disrupted initially because of oxidative stress induced by AOM in the NTS. The ultimate severance of this NTS-RVLM connectivity takes place on shifting oxidative stress to nitrosative stress (formation of peroxynitrite) in the NTS, leading to cessation of action potentials because of the induced cell damage in this medullary site. Together with the formation of peroxynitrite in the RVLM, the BLF power disappeared, signifying that brain death [6, 21-23], which precedes cardiac death, has ensued during the final, pathological stage of HE, a process

that is irreversible. We recognize that both demyelination and axonal injury result in lower anisotropy. Animal studies reported that whereas demyelination often leads to an increase in  $\lambda_{\perp}$  [55], axonal injury is associated with a loss of  $\lambda_{\parallel}$  [56]. It follows that the reduction in  $\lambda_{\parallel}$  and the insignificant changes in  $\lambda_{\perp}$  observed in our study suggested that axonal injury may also underlie the disrupted NTS-RVLM or NTS-NA connectivity. This suggestion, however, awaits further delineation.

## Conclusion

Determination of neural fiber density by DTI has been widely used in studies on neural degeneration [57-59] and brain white matter disorders such as multiple sclerosis, ischemia, traumatic brain injury and cerebral stroke [60-62]. The present study revealed that in addition to morphological evaluations, tractographic analysis of the baroreflex neural circuits offers a hitherto unexplored research dimension on the engagement of baroreflex in cardiovascular functions. In particular, we found that under pathophysiological conditions when the disruption of the functional connectivity between key substrates in the baroreflex circuits is reversible, the associated disease condition is amenable to remedial measurements. On the other hand, fatality ensues when pathophysiological conditions evolve to pathological conditions when the functional connectivity between key substrates in the baroreflex circuits is irreversibly severed. Our findings may therefore be extended to the clinic to aid in the design of alternative therapies based on the principle of reversing a pathophysiological condition to a physiological condition, or preventing a pathophysiological condition from evolving to a pathological condition, using reversibility of disrupted neural circuits as a guide.

## Abbreviations

BP: blood pressure; HR: heart rate; NTS: nucleus tractus solitarius; NA: nucleus ambiguus; CVLM: caudal ventrolateral medulla; RVLM: rostral ventrolateral medulla; MRI: magnetic resonance imaging; DTI: diffusion tensor imaging; ROIs: regions-of-interest; FA: fractional anisotropy; i.c.v.: intracerebroventricular; Ang II: angiotensin II; HE: hepatic encephalopathy; AOM: azoxymethane; SBP: systolic blood pressure; MAP: mean arterial pressure; BLF: low-frequency; BRS: baroreflex sensitivity; ASL: aspartate aminotransferase; ALT: alanine aminotransferase; T-bilirubin: total bilirubin; ROS: reactive oxygen species; RNS: reactive nitrogen species; H&E: hematoxylin and eosin; PVS: persistent vegetative state.

## Supplementary Material

Supplementary Figures S1-S2 and Supplementary Tables 1-4. <http://www.thno.org/v06p0837s1.pdf>

## Acknowledgments

We thank Ms. Shu-Ting Hung and Mr. Chun-Chieh Yu for technical assistance with the MRI/DTI experiments. This work was supported by the National Science Council and Ministry of Science and Technology, Taiwan (MOST-103-2320-B-182A-004-MY3 to C.H.S.; NSC98-2923-B-182A-001-MY3 to A.Y.W.C., J.Y.H.C. and S.H.H.C.; MOST-103-2321-B-182A-001 to S.H.H.C.) and Chang Gung Medical Foundation, Taiwan (CMRPG871341, CLRPG871342, OMRPG8C0021 to S.H.H.C.).

## Competing Interests

The authors declare no competing financial interests.

## References

- Cowley AW Jr, Liard JF, Guyton AC. Role of the baroreceptor reflex in daily control of arterial blood pressure and other variables in dogs. *Circ Res.* 1973; 32: 564-576.
- Thrasher TN. Baroreceptors and the long-term control of blood pressure. *Exp Physiol.* 2004; 89: 331-341.
- Spyer KM. Central nervous mechanisms contributing to cardiovascular control. *J Physiol.* 1994; 474: 1-19.
- Dampney RAL. Functional organization of central pathways regulating the cardiovascular system. *Physiol Rev.* 1994; 74: 323-364.
- Dampney RAL, Horiuchi J. Functional organization of central cardiovascular pathways: studies using c-fos gene expression. *Prog Neurobiol.* 2003; 71: 359-384.
- Chan JYH, Chang AYW, Chan SHH. New insights on brain stem death: from bedside to bench. *Prog Neurobiol.* 2005; 77: 396-425.
- Tsai CY, Su CH, Baudrie V, Laude D, Weng JC, Chang AYW, Chan JYH, Elghozi JL, Chan SHH. Visualizing oxidative stress-induced depression of cardiac vagal baroreflex by MRI/DTI in a mouse neurogenic hypertension model. *Neuroimage.* 2013; 82: 190-199.
- Jiang H, van Zijl PC, Kim J, Pearlson GD, Mori S. DtiStudio: resource program for diffusion tensor computation and fiber bundle tracking. *Comput Methods Programs Biomed.* 2006; 81: 106-116.
- Matkowskyj KA, Marrero JA, Carroll RE, Danilkovich AV, Green RM, Benya RV. Azoxymethane-induced fulminant hepatic failure in C57BL/6mice: characterization of a new animal model. *Am J Physiol.* 1999; 277: G455-G462.
- Béanger M, Côté J, Butterworth RF. Neurobiological characterization of an azoxymethane mouse model of acute liver failure. *Neurochem Int.* 2006; 48: 434-440.
- Guillén JCQ, Gutiérrez JM. Diagnostic methods in hepatic encephalopathy. *Clin Chim Acta.* 2006; 365: 1-8.
- Prakash R, Mullen KD. Mechanisms, diagnosis and management of hepatic encephalopathy. *Nat Rev Gastroenterol Hepatol.* 2010; 7: 515-525.
- Tsai CY, Su CH, Leu S, Chang AYW, Chan JYH, Chan SHH. Endogenous vascular endothelial growth factor produces tonic facilitation of cardiac vagal baroreflex via fetal liver kinase-1 in medulla oblongata. *Int J Cardiol.* 2015; 187: 421-425.
- Li PL, Chao YM, Chan SHH, Chan JYH. Potentiation of baroreceptor reflex response by heat shock protein 70 in nucleus tractus solitarius confers cardiovascular protection during heatstroke. *Circulation.* 2001; 103: 2114-2119.
- Laude D, Baudrie V, Elghozi JL. Applicability of recent methods used to estimate spontaneous baroreflex sensitivity to resting mice. *Am J Physiol Regul Integr Comp Physiol.* 2008; 294: R142-R150.
- Baudrie V, Laude D, Elghozi JL. Optimal frequency ranges for extracting information on cardiovascular autonomic control from the blood pressure and pulse interval spectrograms in mice. *Am J Physiol Regul Integr Comp Physiol.* 2007; 292: R904-R912.
- Montano-Loza AJ. Clinical relevance of sarcopenia in patients with cirrhosis. *World J Gastroenterol.* 2014; 20: 8061-8071.
- Patel D, McPhail MJ, Cobbold JF, Taylor-Robinson SD. Hepatic encephalopathy. *Br J Hosp Med (Lond).* 2012; 73: 79-85.

19. Cash WJ, McConville P, McDermott E, McCormick PA, Callender ME, McDougall NI. Current concepts in the assessment and treatment of hepatic encephalopathy. *Q J Med.* 2010; 103: 9-16.
20. Munoz SJ. Difficult management problems in fulminant hepatic failure. *Semin Liver Dis.* 1993; 13: 395-413.
21. Kuo TBJ, Yien HW, Hseu SS, Yang CCH, Lin YY, Lee LC, Chan SHH. Diminished vasomotor component of systemic arterial pressure signals and baroreflex in brain death. *Am J Physiol.* 1997; 273: H1291-H1298.
22. Yen DHT, Yien HW, Wang LM, Lee CH, Chan SHH. Spectral analysis of systemic arterial pressure and heart rate signals of patients with acute respiratory failure induced by severe organophosphate poisoning. *Crit Care Med.* 2000; 28: 2805-2811.
23. Yien HW, Hseu SS, Lee LC, Kuo TBJ, Lee TY, Chan SHH. Spectral analysis of systemic arterial pressure and heart rate signals as a prognostic tool for the prediction of patient outcome in intensive care unit. *Crit Care Med.* 1997; 25: 258-266.
24. Kim JH, Song SK. Diffusion tensor imaging of the mouse brainstem and cervical spinal cord. *Nature Protocols.* 2013; 8: 409-417.
25. Jennett B, Plum F. Persistent vegetative state after brain damage: a syndrome in search of a name. *Lancet.* 1972; 1: 734-737.
26. The Multi-Society Task Force on PVS. Medical Aspects of the Persistent Vegetative State. *N Engl J Med.* 1994; 330: 1499-1508.
27. The Multi-Society Task Force on PVS. Medical Aspects of the Persistent Vegetative State. *N Engl J Med.* 1994; 330: 1572-1579.
28. The Conference of Medical Royal Colleges and their Faculties in the UK. Diagnosis of brain death. *Br Med J.* 1976; 2: 1187-1188.
29. The Conference of Medical Royal Colleges and their Faculties in the UK. Diagnosis of brain death. *Br Med J.* 1979; 1: 332.
30. Chang AYW, Chan JYH, Chuang YC, Chan SHH. Brain stem death as the vital determinant for resumption of spontaneous circulation after cardiac arrest in rats. *PLoS One.* 2009; 4: e7744.
31. Meeley MP, Ruggiero DA, Ishitsuka T, Reis DJ. Intrinsic gamma-aminobutyric acid neurons in the nucleus of the solitary tract and the rostral ventrolateral medulla of the rat: an immunocytochemical and biochemical study. *Neurosci Lett.* 1985; 58: 83-89.
32. Pallis CA. ABC of brain stem death. *Br Med J. London.* 1983.
33. Wijdicks EFM. Determining brain death in adults. *Neurology.* 1995; 45: 1003-1011.
34. Pallis CA, Prior PF. Guidelines for the determination of death. *Neurology.* 1983; 33: 251-252.
35. Hung TP, Chen ST. Prognosis of deeply comatose patients on ventilators. *J Neurol Neurosurg Psychiatry.* 1995; 58: 75-80.
36. Haupt WF, Rudolf J. European brain death codes: a comparison of national guidelines. *J Neurol.* 1999; 246: 432-437.
37. Chan SHH, Hsu KS, Huang CC, Wang LL, Ou CC, Chan JYH. NADPH oxidase-derived superoxide anion mediates angiotensin II-induced pressor effect via activation of p38 mitogen-activated protein kinase in the rostral ventrolateral medulla. *Circ Res.* 2005; 97: 772-780.
38. Chan SHH, Wu CWJ, Chang AYW, Hsu KS, Chan JYH. Transcriptional upregulation of brain-derived neurotrophic factor in rostral ventrolateral medulla by angiotensin II: significance in superoxide homeostasis and neural regulation of arterial pressure. *Circ Res.* 2010; 107: 1127-1139.
39. Phillips MI. Functions of angiotensin in the central nervous system. *Annu Rev Physiol.* 1987; 49: 413-435.
40. Davissson RL, Oliverio MI, Coffman TM, Sigmund CD. Divergent functions of angiotensin II receptor isoforms in the brain. *J Clin Invest.* 2000; 106: 103-106.
41. Ohinata K, Fujiwara Y, Fukumoto S, Iwai M, Horiuchi M, Yoshikawa M. Angiotensin II and III suppress food intake via angiotensin AT2 receptor and prostaglandin EP4 receptor in mice. *FEBS Lett.* 2008; 582: 773-777.
42. Nakano-Tateno T, Shichiri M, Suzuki-Kemuriyama N, Tani Y, Izumiya H, Hirata Y. Prolonged effects of intracerebroventricular angiotensin II on drinking, eating and locomotor behavior in mice. *Regul Pept.* 2012; 173: 86-92.
43. Thunhorst RL, Lewis SJ, Johnson AK. Role of arterial baroreceptor input on thirst and urinary responses to intracerebroventricular angiotensin II. *Am J Physiol.* 1993; 265: R591-R595.
44. Chan JYH, Cheng HL, Chou JIJ, Li FCH, Dai KY, Chan SHH, Chang AYW. Heat shock protein 60 or 70 activates nitric-oxide synthase (NOS) I- and inhibits NOS II-associated signaling and depresses the mitochondrial apoptotic cascade during brain stem death. *J Biol Chem.* 2007; 282: 4585-4600.
45. Chan, JYH, Wu CHY, Tsai CY, Cheng HL, Dai KY, Chan SHH, Chang AYW. Transcriptional up-regulation of nitric oxide synthase II by nuclear factor- $\kappa$ B at rostral ventrolateral medulla in a rat mevinphos intoxication model of brain stem death. *J Physiol.* 2007; 581: 1293-1307.
46. Yen DHT, Chan JYH, Huang CI, Lee CH, Chan SHH, Chang AYW. Coenzyme Q10 confers cardiovascular protection against acute mevinphos intoxication by ameliorating bioenergetic failure and hypoxia in the rostral ventrolateral medulla of the rat. *Shock.* 2005; 23: 353-359.
47. Yen DHT, Chan JYH, Tseng HP, Huang CI, Lee CH, Chan SHH, Chang AYW. Depression of mitochondrial respiratory enzyme activity in rostral ventrolateral medulla during acute mevinphos intoxication in the rat. *Shock.* 2004; 21: 358-363.
48. Chan JYH, Tsai CY, Wu CHY, Li FCH, Dai KY, Sun EYH, Chan SHH, Chang AYW. Sumoylation of hypoxia-inducible factor-1 $\alpha$  ameliorates failure of brain stem cardiovascular regulation in experimental brain death. *PLoS One.* 2011; 6: e17375.
49. Chan JYH, Chang AYW, Wang LL, Ou CC, Chan SHH. Protein kinase C-dependent mitochondrial translocation of proapoptotic protein Bax on activation of inducible nitric-oxide synthase in rostral ventrolateral medulla mediates cardiovascular depression during experimental endotoxemia. *Mol Pharmacol.* 2007; 71: 1129-1139.
50. Chan SHH, Wu KLH, Wang LL, Chan JYH. Nitric oxide- and superoxide-dependent mitochondrial signaling in endotoxin-induced apoptosis in the rostral ventrolateral medulla of rats. *Free Radic Biol Med.* 2005; 39: 603-618.
51. Sheh YL, Hsu C, Chan SHH, Chan JYH. NADPH oxidase- and mitochondrion-derived superoxide at rostral ventrolateral medulla in endotoxin-induced cardiovascular depression. *Free Radic Biol Med.* 2007; 42: 1610-1623.
52. Wu CHY, Chan JYH, Chan SHH, Chang AYW. A double-edged sword role for ubiquitin-proteasome system in brain stem cardiovascular regulation during experimental brain death. *PLoS One.* 2011; 6: e27404.
53. Li FCH, Yen JC, Chan SHH, Chang AYW. Bioenergetics failure and oxidative stress in brain stem mediates cardiovascular collapse associated with fatal methamphetamine intoxication. *PLoS One.* 2012; 7: e30589.
54. Li FCH, Yen JC, Chan SHH, Chang AYW. Defunct brain stem cardiovascular regulation underlies cardiovascular collapse associated with methamphetamine intoxication. *J Biomed Sci.* 2012; 19: e16.
55. Song SK, Sun SW, Ramsbottom MJ, Chang C, Russel J, Cross AH. Demyelination revealed through MRI as increased radial (but unchanged axial) diffusion of water. *Neuroimage.* 2002; 17: 1429-1436.
56. Mac Donald CL, Dikranian K, Song SK, Bayly PV, Holtzman DM, Brody DL. Detection of traumatic axonal injury with diffusion tensor imaging in a mouse model of traumatic brain injury. *Exp Neurol.* 2007; 205: 116-131.
57. Lim KO, Helpman JA. Neuropsychiatric applications of DTI - a review. *NMR Biomed.* 2002; 15: 587-593.
58. Taber KH. The future for diffusion tensor imaging in neuropsychiatry. *J Neuropsychiatry Clin Neurosci.* 2002; 14: 1-5.
59. Taylor WD, Hsu E, Krishnan KR, MacFall JR. Diffusion tensor imaging: background, potential, and utility in psychiatric research. *Biol Psychiatry.* 2004; 55: 201-207.
60. Horsfield MA, Jones DK. Applications of diffusion-weighted and diffusion tensor MRI to white matter diseases - a review. *NMR Biomed.* 2002; 15: 570-577.
61. Huisman TA. Diffusion-weighted imaging: basic concepts and application in cerebral stroke and head trauma. *Eur Radiol.* 2003; 13: 2283-2297.
62. Pierpaoli C. Water diffusion changes in Wallerian degeneration and their dependence on white matter architecture. *Neuroimage.* 2001; 13: 1174-1185.